Journal of Molecular Structure 1112 (2016) 136–146

Contents lists available at ScienceDirect

Journal of Molecular Structure

journal homepage: http://www.elsevier.com/locate/molstruc

Vibrational and structural observations and molecular docking study on 1-{3-(4-chlorophenyl)-5-[4-(propan-2-yl)phenyl]-4,5-dihydro-1*H*-pyrazol-1-yl}-ethanone

Shana Parveen S [a], Monirah A. Al-Alshaikh [b], C. Yohannan Panicker [a, *], Ali A. El-Emam [c], B. Narayana [d], Vinutha V. Saliyan [d], B.K. Sarojini [e], C. Van Alsenoy [f]

[a] Department of Physics, TKM College of Arts and Science, Kollam, Kerala, India
[b] Department of Chemistry, College of Sciences, King Saud University, Riyadh 11451, Saudi Arabia
[c] Department of Pharmaceutical Chemistry, College of Pharmacy, King Saud University, Riyadh 11451, Saudi Arabia
[d] Department of Studies in Chemistry, Mangalore University, Mangalagangotri, Mangalore, India
[e] Department of Studies in Industrial Chemistry, Mangalore University, Mangalagangotri, Mangalore, India
[f] Department of Chemistry, University of Antwerp, Groenenborgerlaan 171, B-2020 Antwerp, Belgium

ARTICLE INFO

Article history:
Received 27 October 2015
Received in revised form
31 December 2015
Accepted 4 February 2016
Available online 6 February 2016

Keywords:
DFT
FT-IR
FT-Raman
Pyrazole
Molecular docking

ABSTRACT

A combined experimental and theoretical analysis of on molecular structure, vibrational spectra and HOMO-LUMO analysis of 1-{3-(4-chlorophenyl)-5-[4-(propan-2-yl)phenyl]-4,5-dihydro-1*H*-pyrazol-1-yl}-ethanone is reported. The equilibrium geometry and vibrational wavenumbers have been computed using desnity functional B3LYP method with 6−311++G(d) (5D, 7F) as basis set. The nonlinear optical properties were evaluated by the determination of the first and second hyperpolarizabilities of the title compound. HOMO is localized over the whole molecule except the ring PhIII and the CH_3 groups attached to the PhIII while the LUMO is located through out the whole molecule except the CH_3 groups attached with the PhIII and this shows that an eventual charge transfer occurs within the molecule. From the molecular electrostatic potential study, the negative electrostatic potential regions are mainly localized over the carbonyl group, phenyl rings and are possible sites for electrophilic attack and the positive regions are localized over the nitrogen atoms as possible sites for nucleophilic attack. The docked ligand title compound forms a stable complex with kinesin spindle protein (KSP) and gives a binding affinity value of −6.7 kcal/mol the results suggest that the compound might exhibit inhibitory activity against KSP.

1. Introduction

Pyrazoline derivatives possess many biological activities such as anticancer [1] and antioxidant properties [2]. Much attention was given to pyrazoles as antimicrobial agents after the discovery of the natural pyrazole C-glycoside, pyrazofurin which demonstrated abroad spectrum antimicrobial activity [3,4]. Tanitame and co-workers [5–7] reported the antimicrobial activity of several pyrazole derivatives. Lv et al. [8] reported the synthesis and biological evaluation of pyrazole derivatives containing thiourea skeleton as anticancer agents. The authors group reported the vibrational spectroscopic studies of a number of pyrazole derivatives [9–13]. To the best of our knowledge, a detailed description of the spectroscopic behavior of the title compound with the help of vibrational spectral techniques and quantum chemical calculation along with NLO properties has not been given to date. In this work we set out experimental and theoretical investigation of the vibrational spectra of the title compound. A detailed interpretation of the vibrational spectra of the title compound has been made on the basis of the calculated potential energy distribution and redistribution of electron density in various bonding and antibonding orbitals and stabilization energies have been calculated by natural bond orbital analysis to give clear evidence of stabilization orginating from the hyper conjugation of various intra-molecular interactions. HOMO and LUMO energies, the first and second order hyperpolarizabilites of this molecular system are calculated using density functional method. Due to different potent biological

* Corresponding author.
E-mail address: cyphyp@rediffmail.com (C.Y. Panicker).

http://dx.doi.org/10.1016/j.molstruc.2016.02.018
0022-2860/

properties, the molecular docking results are also reported.

2. Experimental details

The title compound was prepared by following the reported procedure [14]. A mixture of (2*E*)-1-(4-chlorophenyl)-3-[4-propan-2-ylphenyl]prop-2-en-1-one (2.85 g, 0.01 mol) and hydrazine hydrate (0.5 mL, 0.01 mol) in 25 mL acetic acid was refluxed for 9 h. The reaction mixture was cooled and poured into ice cold water. The precipitate formed was collected by filtration and purified by recrystallization from ethanol. The FT-IR spectrum (Fig. 1) was recorded using KBr pellets on a DR/Jasco FT-IR 6300 spectrometer with a spectral resolution of 4 cm^{-1}. The FT-Raman spectrum (Fig. 2) was obtained on a Bruker RFS 100/s, Germany and the excitation of the spectrum is with the emission of Nd:YAG laser with a wavelength of 1064 nm, maximal power 150 mW.

3. Computational details

Calculations of the title compound were carried out with the Gaussian09 program [15] using B3LYP/6−311++G(d) (5D, 7F) basis set to predict the molecular structure and vibrational wave numbers and a scaling factor of 0.9613 is used for obtaining a considerably better agreement with experimental data [16]. The theoretical calculations were performed with the hybrid B3LYP functional, i.e. a combination of the Becke's three parameter exchange functional and Lee-Yang-Parr correlation functional [17,18]. The DFT calculations were reported to provide excellent vibrational wavenumber of organic compounds if the calculated wavenumbers are scaled to compensate for the approximate treatment of electron correlation, for basis set deficiencies and for the anharmonicity [19]. The absence of imaginary wavenumbers confirmed that the stationary points correspond to minima on the potential energy surface. Structural parameters corresponding to optimized geometry of the title compound (Fig. 3) with XRD data are given in Table 1. Also the optimized geometry of the title compound without hydrogen atoms is given in Fig. S1 as supporting material. The assignments of the calculated wave numbers are aided by the animation option of the GAUSSVIEW program [20] and the potential energy distribution was calculated by using GAR2PED software package [21].

4. Results and discussion

4.1. IR and Raman spectra

The calculated (scaled) wave numbers, observed IR, Raman bands and assignments are given in Table 2. In the following discussion, the rings, C_{12}–C_{13}–C_{15}–C_{17}–C_{18}–C_{20}, C_6–C_8–C_{11}–N_4–N_3 and C_{22}–C_{23}–C_{25}–C_{27}–C_{28}–C_{30} are designated as PhI, PhII and PhIII, respectively.

For the title compound, the CH_3 stretching modes are assigned at 3002, 2980, 2958, 2914 cm^{-1} in the IR spectrum, 2960, 2938 cm^{-1} in the Raman spectrum and in the range 3032–2906 cm^{-1} theoretically and these modes are expected in the region 2900-3050 cm^{-1} according to literature [22]. The deformation modes of the methyl group of the title compound are assigned as 1425, 1064, 1035, 1023, 892 cm^{-1} in the IR spectrum, 1462, 1441, 1056 cm^{-1} in the Raman spectrum and in the ranges 1465–1352 (scissoring) and 1080-898 cm^{-1} (rocking) theoretically as expected [22]. The stretching vibrations of the CH_2 group and deformation modes of CH_2 group (scissoring, wagging, twisting and rocking modes) appears in the regions 3000 ± 20, 2900 ± 25, 1450 ± 30, 1330 ± 35, 1245 ± 45, 780 ± 55 cm^{-1} respectively [22–24]. The CH_2 stretching modes are observed at 2923 cm^{-1} in the Raman spectrum and at 2926, 2966 cm^{-1} theoretically. The deformation modes of CH_2 are assigned at 1439, 1295, 1220, 1148 cm^{-1} in the IR spectrum, 1146 cm^{-1} in the Raman spectrum

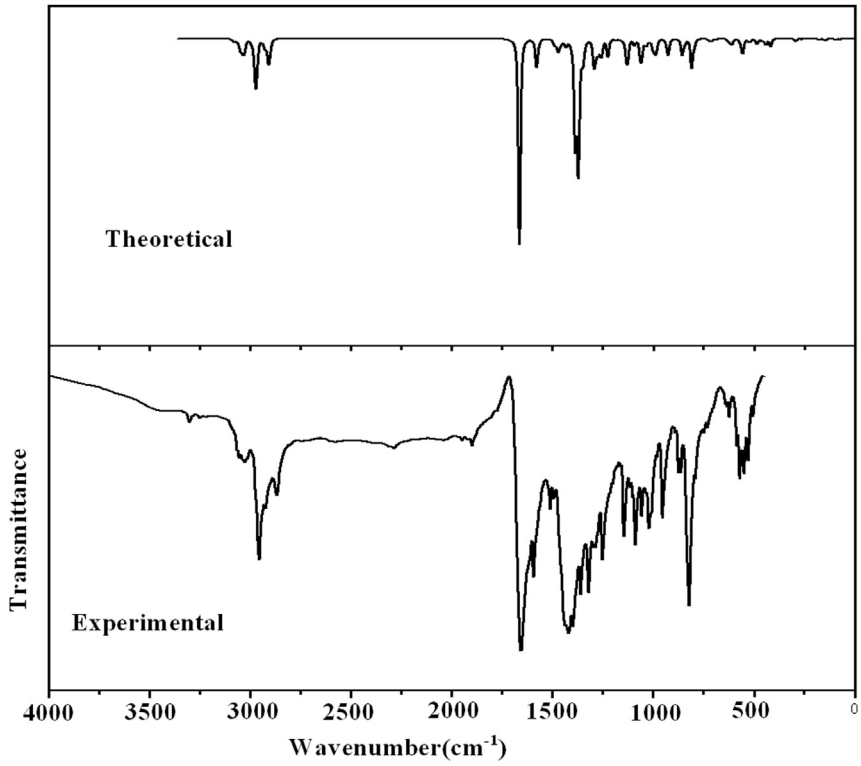

Fig. 1. FT-IR spectrum of 1-{3-(4-chlorophenyl)-5-[4-(propan-2-yl)phenyl]-4,5-dihydro-1H-pyrazol-1-yl}-ethanone.

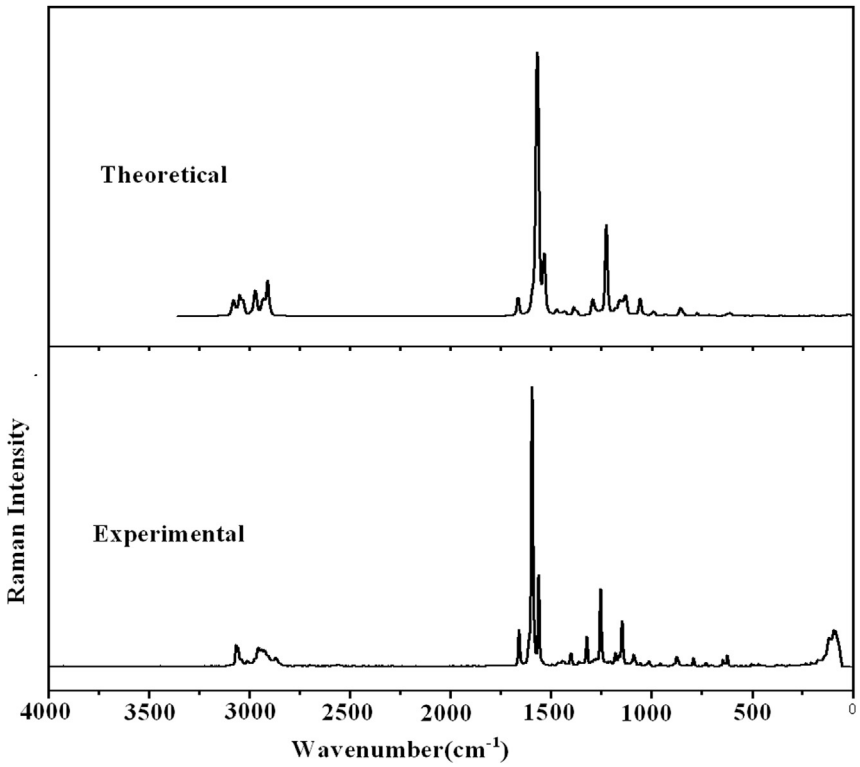

Fig. 2. FT-Raman spectrum of 1-{3-(4-chlorophenyl)-5-[4-(propan-2-yl)phenyl]-4,5-dihydro-1H-pyrazol-1-yl}-ethanone.

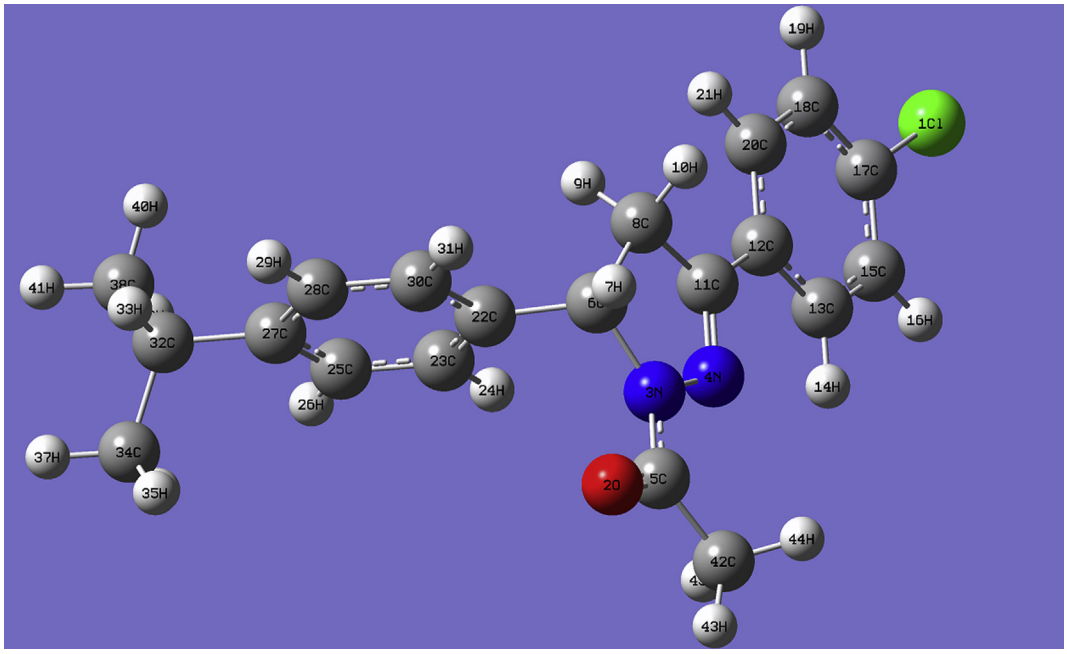

Fig. 3. Optimized geometry of 1-{3-(4-chlorophenyl)-5-[4-(propan-2-yl)phenyl]-4,5-dihydro-1*H*-pyrazol-1-yl}-ethanone.

and in the range 1437–856 cm^{-1} theoretically as expected [22–24].

The bands observed at 1657 cm^{-1} in the IR spectrum, 1662 cm^{-1} in the Raman spectrum and at 1665 cm^{-1} (DFT) are assigned as the stretching modes of C=O and according to literature [25] the stretching mode of C=O is expected in the range 1850–1550 cm^{-1}. The in-plane and out-of-plane bending modes of C=O are reported in the ranges 725 ± 95 and 595 ± 120 cm^{-1} [22]. For the title compound, C=O deformation bands are assigned at 606, 569 cm^{-1} theoretically (DFT).

For the title compound, the C=N stretching mode is assigned at 1579 cm^{-1} theoretically and N–N stretching mode is observed at 1120 cm^{-1} in the IR spectrum and at 1130 cm^{-1} theoretically. The N–N stretching mode is reported at 1108 cm^{-1} in the IR spectrum and at 1116 cm^{-1} theoretically and the C=N stretching mode at

Table 1
Optimized geometrical parameters of 1-{3-(4-Chlorophenyl)-5-[4-(propan-2-yl) phenyl]-4,5-dihydro-1H-pyrazol-1-yl}-ethanone.

Bond lengths (Å) (DFT/XRD[a])			
C17–Cl1	1.7562/1.7442	C5–O2	1.2199/1.2212
N3–N4	1.3727/1.3812	C5–N3	1.3805/1.3572
C6–N3	1.4847/1.4892	C11–N4	1.2891/1.2822
C5C42	1.5124/1.5053	C6–H7	1.0909/1.0000
C6–C8	1.5531/1.5462	C6–C22	1.5167/1.5142
C8–H9	1.092/0.9900	C8–H10	1.0948/0.9900
C8–C11	1.5172/1.5102	C11–C12	1.4641/1.4713
C12–C13	1.4064/1.4053	C12–C20	1.4022/1.3873
C13–H14	1.0834/0.9500	C13–C15	1.3866/1.3863
C15–H16	1.0836/0.9500	C15–C17	1.3953/1.3833
C17–C18	1.3894/1.3763	C18–H19	1.0834/0.9500
C18–C20	1.3928/1.3893	C20–H21	1.0845/0.9500
C22–C23	1.3985/1.3952	C22–C30	1.3935/1.3932
C23–H24	1.0863/0.9500	C23–C25	1.3909/1.3842
C25–H26	1.0859/0.9500	C25–C27	1.4015/1.3943
C27–C28	1.3970/1.3952	C27–C32	1.5213/1.5162
C28–H29	1.0867/0.9500	C28–C30	1.3943/1.3822
C30–H31	1.0864/0.9500	C32–H33	1.0967/1.0000
C32–C34	1.5388/1.5313	C32–C38	1.5386/1.5243
C34–H35	1.0930/0.9800	C34–H36	1.0942/0.9800
C34–H37	1.0944/0.9800	C38–H39	1.0942/0.9800
C38–H40	1.0932/0.9800	C38–H41	1.0943/0.9800
C42–H43	1.0885/0.9800	C42–H44	1.0926/0.9800
C42–H45	1.0916/0.9800		
Bond angles (°) (DFT/XRD)			
N4–N3–C5	122.5/122.6	N4–N3–C6	113.5/113.2
C5–N3–C6	123.5/123.6	N3–N4–C11	109.4/108.7
O2–C5–N3	119.9/120.1	O2–C5–C42	123.7/122.9
N3–C5–C42	116.4/117.1	N3–C6–H7	108.3/109.5
N3–C6–C8	100.8/100.9	N3–C6–C22	113.0/112.2
H7–C6–C8	111.7/109.5	H7–C6–C22	108.9/109.5
C8–C6–C22	113.9/114.9	C6–C8–H9	111.6/111.2
C6–C8–H10	112.2/111.2	C6–C8–C11	102.7/102.6
H9–C8–H10	107.3/109.2	H9–C8–C11	112.4/111.2
H10–C8–C11	110.7/111.2	N4–C11–C8	113.1/114.0
N4–C11–C12	122.0/121.4	C8–C11–C12	125.0/124.5
C11–C12–C13	121.1/120.8	C11–C12–C20	120.7/120.1
C13–C12–C20	118.3/119.0	C12–C13–H14	119.2/120.0
C12–C13–C15	121.0/120.0	H14–C13–C15	119.8/120.0
C13–C15–H16	120.6/120.3	C13–C15–C17	119.4/119.4
H16–C15–C17	120.0/120.3	Cl1–C17–C15	119.5/119.3
Cl1–C17–C18	119.6/118.9	C15–C17–C18	120.9/121.7
C17–C18–H19	120.2/120.6	C17–C18–C20	119.2/118.7
H19–C18–C20	120.6/120.6	C12–C20–C18	121.2/121.1
C12–C20–H21	120.3/119.4	C18–C20–H21	118.6/119.4
C6–C22–C23	121.4/121.8	C6–C22–C30	120.2/120.3
C23–C22–C30	118.3/117.8	C22–C23–H24	119.9/119.5
C22–C23–C25	120.8/120.9	H24–C23–C25	119.3/119.5
C23–C25–H26	118.7/119.3	C23–C25–C27	121.3/121.4
H26–C25–C27	120.0/119.3	C25–C27–C28	117.5/117.3
C25–C27–C32	121.7/123.2	C28–C27–C32	120.8/119.4
C27–C28–H29	119.4/119.3	C27–C28–C30	121.4/121.4
H29–C28–C30	119.2/119.3	C22–C30–C28	120.8/121.0
C22–C30–H31	119.7/119.5	C28–C30–H31	119.5/119.5
C27–C32–H33	106.8/107.3	C27–C32–C34	111.9/110.1
C27–C32–C38	112.0/114.2	H33–C32–C34	107.3/107.3
H33–C32–C38	107.3/107.3	C34–C32–C38	111.1/110.3
C32–C34–H35	111.3/109.5	C32–C34–H36	111.5/109.5
C32–C34–H37	110.7/109.5	H35–C34–H36	107.6/109.5
H35–C34–H37	108.0/109.5	H36–C34–H37	107.5/109.5
C32–C38–H39	111.6/109.5	C32–C38–H40	111.4/109.5
C32–C38–H41	110.7/109.5	H39–C38–H40	107.6/109.5
H39–C38–H41	107.4/109.5	H40–C38–H41	108.0/109.5
C5–C42–H43	108.0/109.5	C5–C42–H44	110.9/109.5
C5–C42–H45	111.5/109.5	H43–C42–H44	109.5/109.5
H43–C42–H45	110.0/109.5	H44–C42–H45	107.0/109.5
Dihedraal angles (°) (DFT/XRD)			
C5–N3–N4–C11	−168.3/−169.1	C6–N3–N4–C11	3.9/2.7
N4–N3–C5–O2	172.9/175.7	N4–N3–C5–C42	−7.0/−3.2
C6–N3–C5–O2	1.5/4.8	C6–N3–C5–C42	−178.4/−174.1
N4–N3–C6–C8	−7.1/−6.1	N4–N3–C6–C22	114.7/116.8
C5–N3–C6–C8	165.0/165.6	C5–N3–C6–C22	−73.2/−71.5
N3–N4–C11–C8	1.5/2.3	N3–N4–C11–C12	−179.6/−179.4
N3–C6–C8–C11	7.1/6.5	C22–C6–C8–C11	−114.2/−114.4
N3–C6–C22–C23	−44.2/−69.6	N3–C6–C22–C30	138.4/110.3
C8–C6–C22–C23	70.1/45.1	C8–C6–C22–C30	−107.4/−135.0
C6–C8–C11–N4	−5.8/−5.9	C6–C8–C11–C12	175.3/175.7
N4–C11–C12–C13	0.9/−3.5	N4–C11–C12–C20	−178.8/177.4
C8–C11–C12–C13	179.7/174.7	C8–C11–C12–C20	−0.1/−4.4
C11–C12–C13–C15	−179.7/−178.2	C20–C12–C13–C15	0.0/0.9
C11–C12–C20–C18	179.7/178.7	C13–C12–C20–C18	−0.1/−0.5
C12–C13–C15–C17	−0.0/−1.1	C13–C15–C17–Cl1	−179.9/−178.5
C13–C15–C17–C18	0.0/0.8	Cl1–C17–C18–C20	179.9/179.0
C15–C17–C18–C20	−0.0/−0.3	C17–C18–C20–C12	0.1/0.2
C6–C22–C23–C25	−177.3/179.7	C30–C22–C23–C25	0.2/−0.2
C6–C22–C30–C28	177.1/179.6	C23–C22–C30–C28	−0.4/−0.5
C22–C23–C25–C27	0.2/0.3	C23–C25–C27–C28	−0.3/0.4
C23–C25–C27–C32	−179.7/−178.1	C25–C27–C28–C30	0.0/−1.1
C32–C27–C28–C30	179.4/177.5	C25–C27–C32–C34	63.1/98.9
C25–C27–C32–C38	−62.4/−26.0	C28–C27–C32–C34	−116.3/−79.6
C28–C27–C32–C38	118.2/155.5	C27–C28–C30–C22	0.3/1.1

[a] XRD data are taken from Ref. [14].

1553 cm^{-1} in the IR spectrum and at 1555 cm^{-1} theoretically for a pyrazole derivative [13].

The vibrations belong C–Cl absorption is obtained in the broad region between 850 and 550 cm^{-1} [26] and the PED analysis give C–Cl stretching mode at 714 cm^{-1} which is in agreement with reported literature [27].

For the title compound, the phenyl CH stretching modes are assigned at 3068, 3051 cm^{-1} in the IR spectrum, 3067, 3058, 3042, 3012 cm^{-1} in the Raman spectrum and in the range 3084–3059 for PhI and 3050-3028 cm^{-1} for PhIII [22] theoretically. The phenyl ring stretching modes are expected in the region 1280-1630 cm^{-1} for para-substituted phenyl rings [13]. For the title compound, the phenyl ring stretching modes are assigned at 1565, 1390 cm^{-1} in the IR spectrum, 1565 cm^{-1} in Raman spectrum, in the range 1579–1269 cm^{-1} theoretically for PhI and at 1593, 1493, 1253 cm^{-1} in the IR spectrum, 1594, 1400, 1255 cm^{-1} in the Raman spectrum, 1593-1255 cm^{-1} theoretically for PhIII. The ring breathing mode, appears as a weak band near 1000 cm^{-1} in mono-, 1,3-di-, and 1,3,5-trisubstituted benzenes [22]. In the otherwise substituted benzenes, however, this vibration is substituent sensitive and difficult to distinguish from the ring in-plane deformation [22]. The ring breathing mode of the para-substituted benzenes with entirely different substituent [28] has been expected in the interval 780-880 cm^{-1}. For the title compound, the PED calculations give the ring breathing modes of the phenyl rings at 856 and 844 cm^{-1} and the reported values are at 873 cm^{-1} in IR spectrum and 861 cm^{-1} theoretically [29]. The in-plane CH deformation bands of the phenyl ring are expected above 1000 cm^{-1} [13] and in the present case, the bands observed at 1280, 1163, 1090 (IR), 1163, 1090 (Raman), 1277, 1161, 1093, 989 (DFT) and 1005 (IR), 1008 (Raman), 1191, 1167, 1131, 1001 cm^{-1} (DFT) are assigned as these modes for PhI and PhIII rings, respectively. The CH out-of-plane deformations of the phenyl ring [22] are observed between 1000 and 700 cm^{-1}. Generally, the CH out-of-plane deformations with the highest wavenumbers have weaker intensity than those absorbing at lower wavenumbers. The γCH vibrations are assigned at 941, 795 (IR), 947 (Raman), 941, 915, 809, 796 cm^{-1} (DFT) and 918, 815 (IR), 923, 919, 811, 807 cm^{-1} (DFT) for rings PhI and PhIII, respectively. The other substituent sensitive modes are also identified and assigned (Table 2). Most of the modes are not pure, but contains significant contributions from other modes also.

4.2. Nonlinear optical properties

The computational method allows the determination of nonlinear optical properties of a molecule as an inexpensive way to

Table 2
Calculated (scaled) wavenumbers, observed IR, Raman bands and assignments of 1-{3-(4-Chlorophenyl)-5-[4-(propan-2-yl)phenyl]-4,5-dihydro-1H-pyrazol-1-yl}-ethanone.

B3LYP/6–311++G(d) (5D, 7F)			IR	Raman	Assignments[a]
υ(cm^{-1})	IRI	RA	υ(cm^{-1})	υ(cm^{-1})	
3084	2.62	118.43	–	–	υCHI(87)
3079	5.71	101.60	–	–	υCHI(97)
3069	1.52	61.29	3068	3067	υCHI(99)
3059	8.45	36.34	–	3058	υCHI(98)
3050	6.13	157.01	3051	–	υCHIII(93)
3045	34.11	100.51	–	3042	υCHIII(92)
3032	12.95	59.97	–	–	υCHIII(64), υCH_3(27)
3032	12.51	80.97	–	–	υCHIII(33), υCH_3(62)
3028	19.23	52.98	–	3012	υCHIII(97)
2993	8.62	35.79	3002	–	υCH_3(99)
2977	33.16	61.25	2980	–	υCH_3(94)
2976	15.79	51.48	–	–	υCHII(54), υCH_2(46)
2974	26.83	35.93	–	–	υCH_3(97)
2969	104.93	227.97	–	–	υCH_3(95)
2966	3.00	57.77	–	–	υCHII(52), υCH_2(43)
2962	0.01	11.69	2958	2960	υCH_3(99)
2937	4.84	176.61	–	2938	υCH_3(100)
2926	19.28	96.24	–	2923	υCH_2(97)
2911	40.13	356.15	2914	–	υCH_3(97)
2906	28.19	7.65	–	–	υCH_3(100)
2900	15.96	84.15	–	–	υCH(94)
1665	502.74	148.60	1657	1662	υC = O(78)
1593	2.01	131.81	1593	1594	υPhIII(74), δCHIII(18)
1579	73.57	62.47	–	–	υC = N(42), υPhI(44)
1569	7.86	3129.81	1565	1565	υPhII(27), υPhI(46)
1555	0.06	12.20	–	–	υPhIII(78)
1536	0.35	490.59	–	–	υPhII(13), υPhI(68)
1491	20.83	1.03	1493	–	δCHIII(22),υPhIII(54)
1474	26.68	41.62	–	–	δCHI(49), υPhI(26)
1465	6.19	3.81	–	–	δCH_3(77)
1460	10.35	13.31	–	1462	δCH_3(85)
1448	3.39	2.38	–	–	δCH_3(84)
1445	0.04	11.37	–	1441	δCH_3(86)
1437	2.48	12.99	1439	–	δCH_2(81)
1434	11.05	10.14	–	–	δCH_3(98)
1429	4.70	20.33	1425	–	δCH_3(92)
1406	10.55	2.82	–	1400	υPhIII(48),δCHIII(30)
1388	248.45	63.86	1390	–	υPhI(52), υCN(13), δCHI(23)
1377	3.60	1.79	–	–	δCH_3(93)
1372	309.29	32.98	1368	1368	υCN(18), υPhI(21), δCH_3(10), δCHI(15)
1356	6.60	0.10	–	–	δCH_3(93)
1352	52.88	1.53	–	–	δCH_3(76)
1342	11.86	1.11	–	–	υCC(46), δCHII(10), δCHIII(22)
1329	0.37	4.82	1327	1324	υCC(32), υPhIII(23)
1299	1.82	8.39	–	–	δCH(44)
1293	94.88	165.24	1295	–	δCH_2(46),υPhII(10), υCN(10), δCHI(10)
1277	19.60	30.35	1280	–	δCHI(56), δCHII(22)
1275	12.44	2.55	–	–	δCHII(44), δCHI(18)
1269	24.62	10.83	–	–	υPhI(73)
1256	31.97	13.27	–	1255	δCHII(26)
1255	8.04	9.98	1253	1255	υPhIII(52), δCHII(13)
1226	45.03	700.17	1220	–	δCH_2(47), υCC(19)
1191	1.86	18.86	–	–	υCC(36), υPhIII(19), δCHIII(11)
1181	1.14	35.10	1178	1179	υCC(33), υPhIII(30)
1167	1.79	16.01	–	–	υPhIII(10),δCHIII(70)
1161	1.14	131.86	1163	1163	υPhI(15), δCHI(76)
1146	4.54	93.54	1148	1146	δCH_2(54), δCHII(20)
1131	19.57	39.27	–	–	δCH_3(25),δCHIII(42), υPhIII(10)
1130	73.52	163.39	1120	–	δCHII(17), υNN(56)
1095	9.23	3.24	1101	–	δCHIII(15), υPhIII(13), δCHI(20), υPhI(13)
1093	7.63	10.87	1090	1090	υPhIII(11), υPhI(17), δCHI(44), δCHIII(10)
1080	1.21	5.64	–	–	δCH_3(42), υCC(50)

Table 2 (*continued*)

B3LYP/6−311++G(d) (5D, 7F)			IR	Raman	Assignments[a]
υ(cm^{-1})	IRI	RA	υ(cm^{-1})	υ(cm^{-1})	
1062	56.93	14.30	1064	–	δCH_3(41), υPhI(38)
1057	22.65	117.48	–	1056	δCH_3(49), υPhI(20)
1037	20.56	13.69	1035	–	δCH_3(48), υPhII(14)
1021	5.98	2.36	1023	–	δCH_3(80), γC = O(17)
1001	24.82	6.73	1005	1008	υPhII(22), υPhI(13), δCHII(40)
997	11.14	10.85	–	–	δPhII(43), υPhII(17)
989	9.99	26.5	–	–	δCHI(53), υPhI(11)
985	28.60	2.64	982	–	δPhI(15), υPhII(30), δCH_2II(18)
941	1.51	2.39	941	947	γCHI(65)
935	3.62	3.46	–	–	δCH_2II(20),γCHI(31), υPhII(11)
929	0.15	4.84	–	–	δCH_3(35), υCC(31), γCHIII(11)
928	37.68	5.77	–	–	δCH_3(25), υCC(25), υPhII(23)
923	0.06	0.65	–	–	γCHIII(83)
919	2.61	0.26	918	–	γCHIII(73),τPhIII(20)
915	0.16	0.89	–	–	γCHI(78), τPhI(12)
898	0.32	0.85	892	–	δCH_3(74), δCC(15)
864	1.07	7.33	864	870	δCH_3(14), υCC(67)
856	42.32	58.69	–	–	δCH_2(39),υPhII(45)
844	9.09	19.34	–	–	δPhII(28), υPhI(44)
811	35.95	0.41	815	–	γCHIII(55)
809	45.05	0.72	–	–	γCHI(57)
807	0.29	0.27	–	–	γCHIII(98)
796	11.72	0.34	795	–	γCHI(87)
775	0.35	23.52	–	780	δPhIII(22), υCC(12)
733	1.12	0.63	731	729	τPhIII(67), γCC(23)
714	10.73	9.97	–	–	τPhI(25), υCCl(48)
698	0.99	2.11	700	–	τPhI(66), γCC(12), γCCl(10)
690	2.11	3.53	–	–	τPhI(15), υCC(19)
630	3.16	8.62	631	–	τPhIII(58)
624	6.94	4.69	624	622	τPhI(49), τPhIII(18)
613	13.82	18.08	–	–	τPhI(25), δCH_2II(11)
606	3.12	8.17	–	–	δ_C = O(44), δCC(21)
569	7.37	1.79	–	–	γC = O(53), δCH_3(16)
558	35.55	1.21	555	–	τPhIII(19), γCC(36)
547	3.74	1.38	–	–	τPhII(11), γCC(11), δPhIII(11), δCC(10)
524	12.46	2.21	527	–	τPhI(21), γCC(31), γCCl(12)
487	12.54	6.12	487	–	τPhIII(31), υCCl(14)
477	2.61	0.57	–	–	τPhII(21), τPhI(12), δCC(14)
457	5.77	5.58	–	460	τPhII(30), τPhI(31), δCC(14)
441	15.58	1.46	–	–	τPhIII(26), δCCl(14), δ_C = O(10)
419	19.83	0.98	–	–	δCCl(10), δCC(56)
401	0.02	0.06	–	–	τPhI(80)
399	0.25	0.08	–	–	τPhIII(81)
363	0.71	0.95	–	368	τPhIII(30), γCC(17), γCCl(22)
354	0.50	1.66	–	–	δCC(26), δ_C = O(20)
336	0.43	0.73	–	–	δCC(36), τPhII(28)
294	7.32	0.57	–	–	δCCl(44), τPhIII(10), δCC(17)
269	0.59	0.62	–	–	δCC(28), δPhI(29)
266	1.37	0.037	–	–	τCH_3(31), δCC(40)
246	0.72	0.63	–	–	τPhIII(24), δCCl(18), γCC(20)
237	0.48	0.59	–	235	τCH_3(37), δCC(12), γCN(10)
224	0.03	0.20	–	–	τCH_3(92)
209	0.54	2.40	–	208	γCC(37), γCN(32)
192	1.25	1.50	–	–	δPhI(20), δCC(18), τPhI(30)
176	3.36	0.83	–	175	δCN(30), δCC(20)
148	4.52	2.93	–	–	γCC(44), τPhII(14)
141	1.11	0.23	–	–	δCC(48), γCN(18)

(*continued on next page*)

Table 2 (*continued*)

B3LYP/6–311++G(d) (5D, 7F)			IR	Raman	Assignments[a]
υ(cm^{-1})	IRI	RA	υ(cm^{-1})	υ(cm^{-1})	
119	0.04	0.23	–	121	$\delta CH_3(19)$, $\tau CH_3(75)$
95	3.89	0.83	–	–	δCN(60), τPhI(10)
83	0.24	2.72	–	–	τPhIII(21), γCN(22), γCC(11)
74	1.57	0.41	–	–	δCC(58), δCN(10)
60	0.64	0.10	–	–	τPhI(17), γCC(27), τPhII(16)
48	0.07	3.58	–	–	τCC(51), γCN(16)
37	0.29	1.00	–	–	γCN(24), τCC(42)
27	0.06	6.53	–	–	τCC(52), τPhII(10), γCC(15)
13	0.02	4.37	–	–	τPhII(47), γCN(20)
11	0.07	2.57	–	–	τCC(45), τPhII(19)

[a] υ-stretching; δ-in-plane deformation; γ-out-of-plane deformation; τ-torsion; PhI-C12-C13-C15-C17-C18-C20 phenyl ring; PhII-C6-C8-C11-N4-N3 ring; PhIII-C22-C30-C28-C27-C25-C23 phenyl ring; potential energy distribution (%) is given in brackets in the assignment column; IR_I-IR intensity; R_A-Raman activity.

design the molecules by analyzing their potential before synthesis and to determine higher order hyperpolarizability values and significant contributions to the search of new nonlinear optical materials with potential applications in advanced technologies can be made with the accurate theoretical determination of hyperpolarizability values [30]. In order to investigate the relationships among molecular structures and nonlinear optical properties, the polarizabilities and first order hyperpolarizabilities of the title compound was calculated using DFT-B3LYP method based on the finite field approach. The dipole moment μ, the mean polarizability α_0 are calculated using Gaussian 09 software and are found to be 2.342 Debye and 4.22×10^{-23} e.s.u respectively. The first order hyperpolarizability of the title compound is calculated and is found to be 6.11×10^{-30} e.s.u and comparable with that of similar derivatives [11–13] and 47 times that of the standard NLO material urea (0.13×10^{-30} e.s.u) [31]. The average second hyperpolarizability is $\langle\gamma\rangle = (\gamma_{xxxx} + \gamma_{yyyy} + \gamma_{zzzz} + 2\gamma_{xxyy} + 2\gamma_{xxzz} + 2\gamma_{yyzz})/5$ [32]. The theoretical second order hyperpolarizability was calculated using the Gaussian09 software and is equal to -30.91×10^{-37} e.s.u. We conclude that the title compound and its derivatives are an attractive object for future studies of nonlinear optical properties.

4.3. Frontier molecular orbital analysis

Molecular orbitals and their properties such as energy are very useful for physicists and chemists and for predicting the most reactive position in π-electron systems and explain several types of reaction in conjugated systems [33]. The pictorial representation of the HOMO and the LUMO is shown in Fig. 4. The HOMO lies at −7.540 eV and whereas the LUMO is located at −4.799 eV and HOMO is delocalized over the whole molecule except the PhIII, CH_3 groups attached to the PhIII while the LUMO is located through out the whole molecule except the CH_3 groups attached with the PhIII. This shows that an eventual charge transfer occurs within the molecule, and that the frontier orbital energy gap is 2.743 eV. By using the HOMO and LUMO energy values, the global chemical reactivity descriptors such as hardness, chemical potential, electronegativity and electrophilicity index as well as local reactivity can be defined [34]. Hardness (η), chemical potential (μ) and electronegativity (χ) are defined using Koopman's theorem as $\eta = (I\text{-}A)/2 = 2.372$ eV, $\mu = -(I + A)/2 = -6.169$ eV and $\chi = (I + A)/2 = 6.169$ eV, where A and I are the ionization potential and electron affinity of the molecule. $I = -E_{HOMO} = 7.540$ eV and $A = -E_{LUMO} = 4.797$ eV. Parr et al. [35] have defined a descriptor to quantify the global electrophilic power of the molecule as the electrophilicity index, $\omega = \mu^2/2\eta = 8.022$ eV. It is seen that the chemical potential of the title compound is negative and it means that the compound is stable [36].

4.4. Molecular electrostatic potential

To predict reactive sites for electrophilic and nucleophilic attack in the investigated molecule, the MEP surface is plotted for the title compound at DFT level [37]. Fig. 5 shows the electrostatic potential contour map of the title compound. The different values of the electrostatic potential at the surface are represented by different colors; red represents regions of most electro negative electrostatic potential, blue represents regions of most positive electrostatic potential and green represents regions of zero potential. The electrostatic potential increases in the order red < orange < yellow < green < blue [38]. As can be seen from the Fig. 5, the negative electrostatic potential regions are mainly localized over the carbonyl group and the phenyl rings, PhI and PhIII and are possible sites for electrophilic attack. The positive regions are localized over the nitrogen atoms as possible sites for nucleophilic attack.

4.5. Natural bond orbital analysis

The natural bond orbitals (NBO) calculations were performed using NBO 3.1 program [39] as implemented in the Gaussian09 package at the DFT/B3LYP level in order to understand various second-order interactions and these interactions are given in Table 3. The second-order perturbation theory analysis of Fock-matrix in NBO basis shows strong intra-molecular hyper conjugative interactions are formed by orbital overlap between n(O), n(N), n(Cl) and σ*(C–N), π*(C–C), π*(C–O), σ*(C–C), bond orbitals which result in intra-molecular charge transfer causing stabilization of the system.

The various conjugative interactions are: C_{17}–C_{18} from Cl_1 of $n_3(Cl_1) \rightarrow \sigma^*(C_{17}–C_{18})$, N_3–C_5 from O_2 of $n_2(O_2) \rightarrow \sigma^*(N_3–C_5)$, C_5–O_2 from N_3 of $n_1(N_3) \rightarrow \pi^*(C_5–O_2)$ with electron densities, 0.38493, 0.08464, 0.26309e and stabilization energies 12.26, 27.67, 54.49 kJ/mol. The NBO also analysis describes the bonding in terms of the orbitals with high and low p characters and the orbitals with considerable p characters are: $n_2(Cl_1)$, $n_2(O_2)$ with higher energy orbital −0.32125, −0.23562a.u and low occupation number 1.92811, 1.86601; while the orbitals, $n_2(Cl_1)$, $n_1(O_2)$ occupy lower energy orbitals, −0.92046, −0.66432a.u with high occupation numbers, 1.99338, 1.97678. Thus, a very close to pure p-type lone pair orbital participates in the electron donation to the $n_3(Cl_1) \rightarrow$

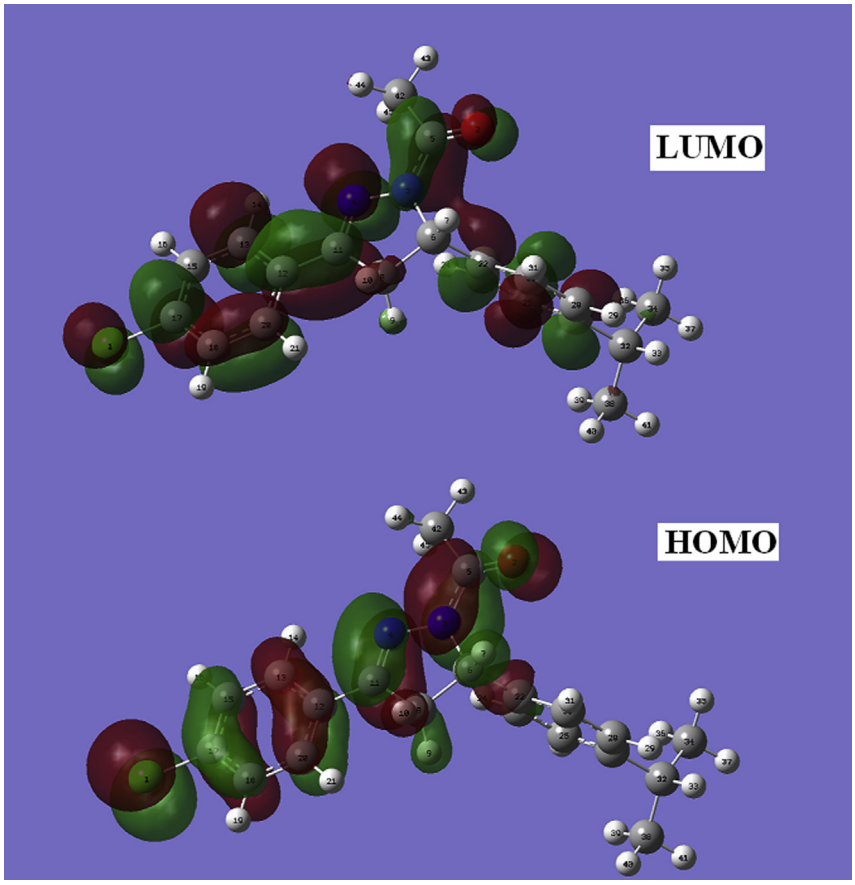

Fig. 4. HOMO-LUMO plots of 1-{3-(4-chlorophenyl)-5-[4-(propan-2-yl)phenyl]-4,5-dihydro-1H-pyrazol-1-yl}-ethanone.

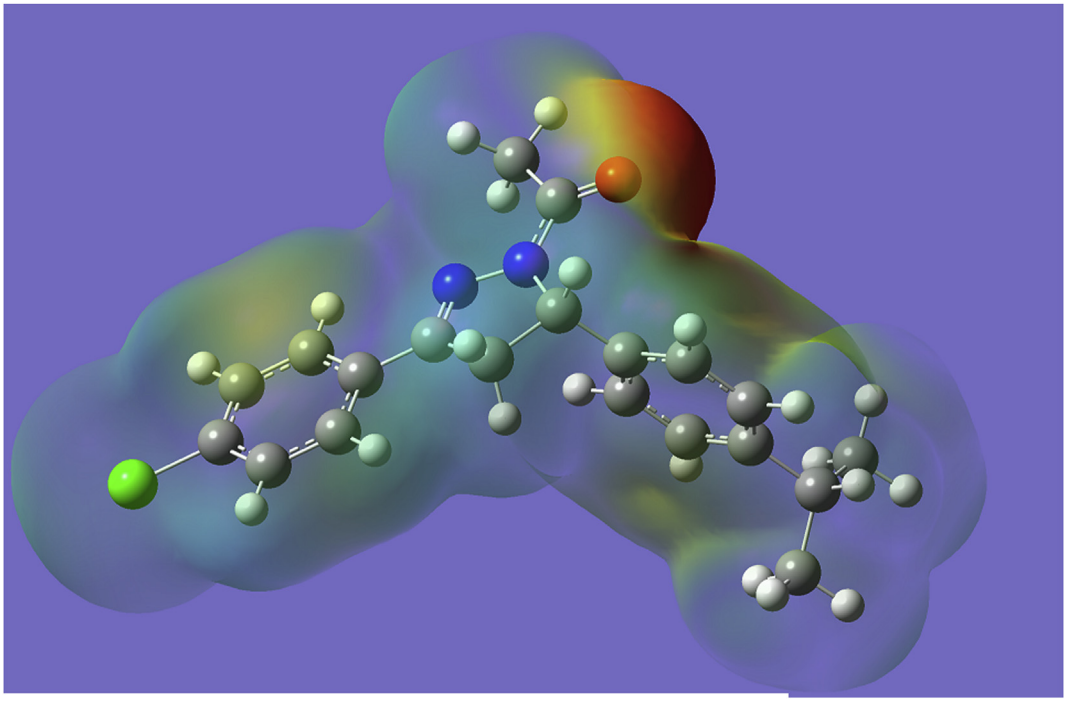

Fig. 5. MEP plot of 1-{3-(4-chlorophenyl)-5-[4-(propan-2-yl)phenyl]-4,5-dihydro-1H-pyrazol-1-yl}-ethanone.

$\sigma^*(C_{17}-C_{18})$, $n_2(O_2)\rightarrow\sigma^*(N_3-C_5)$ and $n_1(N_3)\rightarrow\pi^*(C_5-O_2)$ interactions in the compound. The results are tabulated in Table 4.

Table 3
Second-order perturbation theory analysis of Fock matrix in NBO basis corresponding to the. intra-molecular bonds of the title compound.

Donor(i)	Type	ED/e	Acceptor(j)	Type	ED/e	E(2)[a]	E(j)–E(i)[b]	F(ij)[c]
N3–C5	σ	1.98960	N3–C6	σ*	0.05627	1.19	1.14	0.033
_	–		N4–C11	σ*	0.01346	1.51	1.42	0.041
N3–C6	σ	1.98960	N3–C5	σ*	0.08464	1.37	1.18	0.037
_	–		C5–C42	σ*	0.05383	2.19	1.12	0.045
_	–		C22–C30	σ*	0.02153	1.22	1.32	0.036
N4–C11	π	1.91656	C12–C20	π*	0.38375	9.28	0.36	0.056
C5–C42	σ	1.91656	N3–C6	σ*	0.05627	4.23	0.95	0.057
C6–C22	σ	1.97284	N3–N4	σ*	0.02994	1.04	0.99	0.029
_	–		C22–C23	σ*	0.02393	2.14	1.21	0.045
_	–		C22–C30	σ*	0.02153	2.09	1.22	0.045
_	–		C23–C25	σ*	0.01376	2.05	1.22	0.045
_	–		C28–C30	σ*	0.01355	2.00	1.22	0.044
C8–C11	σ	1.97807	N3–C6	σ*	0.05627	1.71	0.94	0.036
_	–		C11–C12	σ*	0.03207	1.53	1.12	0.037
_	–		C12–C13	σ*	0.02244	2.42	1.19	0.048
C11–C12	σ	1.97188	N3–N4	σ*	0.02994	3.24	1.04	0.052
_	–		N4–C11	σ*	0.01346	2.16	1.27	0.047
_	–		C12–C13	σ*	0.02244	2.56	1.24	0.050
_	–		C12–C20	σ*	0.02128	2.45	1.24	0.049
_	–		C13–C15	σ*	0.01469	1.79	1.26	0.043
_	–		C18–C20	σ*	0.01481	1.97	1.25	0.044
C15–C17	σ	1.98131	C13–C15	σ*	0.01469	2.53	1.31	0.051
_	–		C17–C18	σ*	0.02669	3.86	1.29	0.063
C17–C18	σ	1.98128	C15–C17	σ*	0.02730	3.84	1.29	0.063
_	–		C18–C20	σ*	0.01481	2.55	1.30	0.052
_	π	1.67876	C12–C20	π*	0.38375	18.52	0.30	0.067
_	–		C13–C15	π*	0.28612	18.11	0.30	0.067
LPCl1	σ	1.99338	C15–C17	σ*	0.02730	1.26	1.47	0.039
_	–		C17–C18	σ*	0.02669	1.27	1.48	0.039
_	π	1.97307	C15–C17	σ*	0.02730	3.88	0.87	0.052
_	–		C17–C18	σ*	0.02669	3.88	0.88	0.052
_	n	1.92811	C17–C18	π*	0.38493	12.26	0.33	0.062
LPO2	σ	1.97678	N3–C5	σ*	0.08464	1.54	1.12	0.038
_	–		C5–C42	σ*	0.05383	2.30	1.06	0.044
_	π	1.86601	N3–C5	σ*	0.08464	27.67	0.69	0.125
_	–		C5–C42	σ*	0.05383	19.55	0.63	0.101
LPN3	σ	1.64151	O2–C5	π*	0.26309	54.49	0.29	0.114
_	–		N4–C11	π*	0.21771	27.04	0.27	0.080
_	–		C6–C22	σ*	0.03215	5.05	0.68	0.057
LPN4	σ	1.93155	N3–C6	σ*	0.05627	7.90	0.72	0.067
_	–		C8–C11	σ*	0.03374	8.23	0.80	0.073
_	–		C11–C12	σ*	0.03207	1.10	0.90	0.028

[a] E(2) means energy of hyper-conjugative interactions (stabilization energy in kJ/mol).
[b] Energy difference (a.u) between donor and acceptor i and j NBO orbitals.
[c] F(i,j) is the Fock matrix elements (a.u) between i and j NBO orbitals.

4.6. Molecular docking

Pyrazoles emerged as a powerful pharmacophore scaffold and they have been extensively used to design various kinase inhibitors [40]. Pyrazole derivatives inhibit Aurora kinases, thus inducing apoptosis in tumor cells [41]. ENMD-2076 is an orally-active analog of tozasertib, based on the 3-aminopyrazole template, and a potent inhibitor of Aurora A kinase and of other cancer-related kinases. ENMD-2076 has demonstrated significant preclinical activity and is tested in multiple clinical studies in order to develop specific antitumor therapies [42]. Barasertib is also an anticancer 3-aminopyrazole derivative acting through Aurora B kinase inhibition [43]. Pyrazole derivatives showed their anti-proliferative activity in human ovarian adenocarcinoma A2780 cells, human lung carcinoma A549 cells, and murine P388 leukemia cells [44]. The Kinesin superfamily is a protein belongs to a class of motor proteins; it plays an essential roles in mitosis of eukaryotic cells, such as mitotic spindle function, targets in the anti-mitotic cancer therapeutics [45]. High resolution crystal structure of kinesin spindle protein (KSP) reductase was downloaded from the protein data bank website (PDB ID: 1YRS) and all molecular docking calculations were performed on Auto Dock-Vina software [46]. The protein was prepared for docking by removing the co-crystallized ligands, waters and co-factors and the Auto Dock Tools graphical user interface was used to calculate Kollman charges and polar hydrogens. The ligand was prepared for docking by minimizing its energy at B3LYP/6–311++G(d) (5D, 7F) level of theory and partial charges were calculated by Geistenger method. The active site of the enzyme was defined to include residues of the active site within the grid size of 40 Å × 40 Å × 40 Å. The most popular algorithm, Lamarckian Genetic Algorithm (LGA) available in Autodock was employed for docking and the docking protocol was tested by

Table 4
NBO results showing the formation of Lewis and non-Lewis orbitals.

Bond(A-B)	ED/e[a]	EDA%	EDB%	NBO	s%	p%
σ N3–C5	1.98960	64.34	35.66	0.8021($sp^{1.62}$)N+	38.14	61.86
_	−0.82503	–	–	0.5972($sp^{2.31}$)C	30.16	69.84
σ N3–C6	1.98213	62.27	37.73	0.7891($sp^{2.04}$)N+	32.91	67.09
_	−0.72387	–	–	0.6143($sp^{3.96}$)C	20.13	79.87
π N4–C11	1.91656	56.34	43.66	0.7506($sp^{1.00}$)N+	0.01	99.99
_	−0.33405	–	–	0.6607($sp^{1.00}$)C	0.01	99.99
σ C5–C42	1.98563	49.27	50.73	0.7019($sp^{1.67}$)C+	37.39	62.61
_	−0.63313	–	–	0.7123($sp^{2.78}$)C	26.42	73.58
σ C6–C22	1.97284	50.41	49.59	0.7100($sp^{2.43}$)C+	29.13	70.87
_	−0.62628	–	–	0.7042($sp^{2.24}$)C	30.78	69.22
σ C8–C11	1.97807	50.48	49.52	0.7105($sp^{2.94}$)C+	25.34	74.66
_	−0.63124	–	–	0.7037($sp^{2.03}$)C	32.98	67.02
σ C11–C12	1.97188	49.51	50.49	0.7036($sp^{1.77}$)C+	36.15	63.85
_	−0.67978	–	–	0.7106($sp^{2.12}$)C	32.03	67.97
σ C15–C17	1.98131	49.13	50.87	0.7009($sp^{1.92}$)C+	34.23	65.77
_	−0.72850	–	–	0.7132($sp^{1.59}$)C	38.64	61.36
σ C17–C18	1.98128	50.76	49.24	0.7125($sp^{1.57}$)C+	38.83	61.17
_	−0.73293	–	–	0.7017($sp^{1.90}$)C	34.51	65.49
n1Cl1	1.99338	–	–	$sp^{0.22}$	82.26	17.74
_	−0.92046					
n2Cl1	1.97307	–	–	$sp^{1.00}$	0.00	100.00
_	−0.32246					
n3Cl1	1.92811	–	–	$sp^{1.00}$	0.00	100.00
_	−0.32125					
n1O2	1.97678	–	–	$sp^{0.71}$	58.35	41.65
_	−0.66432					
n2O2	1.86601	–	–	$sp^{1.00}$	0.00	100.00
_	−0.23562					
n1N3	1.64151	–	–	$sp^{99.99}$	0.42	99.58
_	−0.26035					
n1N4	1.93155	–	–	$sp^{1.87}$	34.80	65.20
_	−0.40573	–	–	–	–	–

[a] ED/e is expressed in a.u.

extracting co-crystallized inhibitor from the protein and then docking the same. The docking protocol predicted the same conformation as was present in the crystal structure with RMSD value well within the reliable range of 2 Å [47]. Amongst the docked conformations, one which binded well at the active site was analyzed for detailed interactions in Discover Studio Visualizer 4.0 software. The ligand binds at the active site of the substrate (Fig. 6 and Fig. S2 (supporting material)) by weak non-covalent interactions. Amino acids Arg138 forms H-bond interaction with pyrazole ring and other hydrophobic interactions are shown in Fig. S3 (supporting material). The docked ligand title compound forms a stable complex with KSP and gives a binding affinity (ΔG in kcal/mol) value of −6.7 (Table 5). These preliminary results suggest that the compound might exhibit inhibitory activity against KSP.

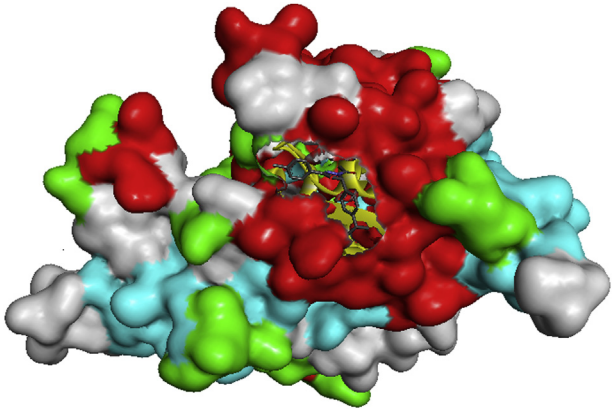

Fig. 6. Pictorial representation of the ligand embedded in the active site of KSP.

4.7. Geometrical parameters

The N–N bond length (DFT/XRD) is reported as 1.3755/1.3886 Å [13] and in the present case the N–N bond length is 1.3727/1.3812 Å. The C–N bond lengths (DFT/XRD) within the RingII are C_{11}–N_4 = 1.2891/1.2822 Å, C_6–N_3 = 1.4847/1.4892 Å and these values show an excellent agreement between the theoretical and experimental results for this fragment of the title compound whereas the corresponding reported bond lengths are 1.2879/1.2923 Å and 1.4825/1.4866 Å [13]. The C_5–N_3 bond length 1.3805/1.3572 Å is significantly longer than C=N double bond (1.22 Å) [48], suggesting that some multiple bond character is present and the corresponding reported value is 1.3677/1.3458 Å [13]. In the present case, the C=O bond length (DFT/XRD) is 1.2199/1.2212 Å and Mary et al. [13] reported the C=O bond length as 1.2144/1.2255 Å. The C–C bond lengths (DFT/XRD) in the phenyl rings are in the range 1.3866–1.4064/1.3763–1.4053 Å for RingI and 1.3909–1.4015/1.3822–1.3952 Å for RingIII. Both the phenyl rings are regular hexagon with bond lengths somewhere in between the normal values for a single (1.54 Å) and a double (1.33 Å) bond [49]. According to our calculations, at C_{22} position, the bond angles, C_{23}–C_{22}–C_{30} = 118.3°, C_{23}–C_{22}–C_6 = 121.4° and C_{30}–C_{22}–C_6 = 120.2° and this asymmetry is due to the interaction between the ring III and II, which are in agreement with XRD results. Similarly at C_{11} postilion, the angles, N_4–C_{11}–C_8 is reduced by 6.9°, N_4–C_{11}–C_{12} is increased by 2° and C_8–C_{11}–C_{12} is increased by 5° from 120°, which is due to the interaction between the chlorophenyl ring RingI and the RingII. At C_{27} position, the bond angles C_{28}–C_{27}–C_{25} = 117.5° and C_{25}–C_{27}–C_{32} = 121.7° and this asymmetry is due to the interaction between the adjacent methyl groups and the ring RingIII. Similarly at N_3, the bond angles are C_6–N_3–N_4 = 113.5°, C_6–N_3–C_5 = 123.5° and N_4–N_3–C_5 = 122.5° and this values show the interaction between pyrazole and the adjacent moieties. The pyrazole ring, RingII is tilted from the phenyl ring, RingIII as is evident from the torsion angles, C_{30}–C_{22}–C_6–N_3 = 138.4°, C_{30}–C_{22}–C_6–C_8 = −107.4°, C_{23}–C_{22}–C_6–C_8 = 70.1° and C23–C_{22}–C_6–N_3 = −44.2°.

5. Conclusion

The vibrational spectroscopic studies of 1-{3-(4-chlorophenyl)-5-[4-(propan-2-yl)phenyl]-4,5-dihydro-1*H*-pyrazol-1-yl}-ethanone were reported theoretically and experimentally. The complete vibrational are done using potential energy distribution analysis.

Table 5
The binding affinity values of different poses of the titlecompound predicted by Autodock Vina.

Mode	Affinity (kcal/mol)	Distance from best mode (Å)	
		RMSD l.b.	RMSD u.b.
1	−6.7	0.000	0.000
2	−6.6	16.304	17.445
3	−6.3	5.472	8.545
4	−6.3	3.146	4.642
5	−6.2	15.637	16.743
6	−6.2	6.179	10.763
7	−6.1	27.855	31.328
8	−6.1	17.632	19.103
9	−6.0	17.975	21.575

NBO analysis predicts the strong intra-molecular hyper conjugative interaction between different orbitals and MEP predicts the most reactive part in the molecule. The calculated first hyerpolarizability is compared with the reported value of similar derivative and hence the title compound and its derivatives are an attractive object for future studies in nonlinear optics. From the molecular docking studies, the ligand binds at the active site of the substrate by weak non-covalent interactions and the amino acids Arg138 forms H-bond interaction with pyrazole ring and the results suggest that the compound might exhibit inhibitory activity against KSP.

Acknowledgments

The authors would like to extend their sincere appreciation to the Deanship of Scientific Research at King Saud University for funding this work through the Research Group Project No. PRG-1436-23.

Appendix A. Supplementary data

Supplementary data related to this article can be found at http://dx.doi.org/10.1016/j.molstruc.2016.02.018.

References

[1] F. Manna, F. Chimenti, F. Fioravanti, A. Bolasco, D. Seeci, P. Chimenti, C. Ferlini, G. Scambia, Bioorg. Med. Chem. Lett. 15 (2005) 4632–4635.
[2] S. Samshuddin, B. Narayana, B.K. Sarojini, M.T.H. Khan, H.S. Yathirajan, C.G. Darsan Raj, R. Ragavendra, Med. Chem. Res. 21 (2012) 2012–2022.
[3] S.G. Kucukguzel, S. Rollas, H. Erdeniz, M. Kiraz, A.C. Ekinci, A. Vidin, Eur. J. Med. Chem. 35 (2000) 761–771.
[4] M.J. Genin, D.A. Allwine, D.J. Anderson, M.R. Barbachyn, D.E. Emmert, S.A. Gamon, D.R. Graber, K.C. Grega, J.B. Hester, D.K. Hutchinson, J. Morris, R.J. Reischer, C.W. Ford, G.E. Zurenko, J.C. Hamel, R.D. Schaadt, D. Stapert, B.H. Yagi, J. Med. Chem. 43 (2000) 953–970.
[5] A. Tanitame, Y. Oyamada, K. Ofuji, Y. Kyoya, K. Suziki, H. Ito, M. Kawasaki, K. Nagai, M. Wachi, J. Yamagishi, Bioorg. Med. Chem. Lett. 14 (2004) 2857–2862.
[6] A. Tanitame, Y. Oyamada, K. Ofuji, K. Suziki, H. Ito, M. Kawasaki, M. Wachim, J. Yamagishi, Bioorg. Med. Chem. Lett. 14 (2004) 2863–2866.
[7] A. Tanitame, Y. Oyamada, K. Ofuji, M. Fujimoto, N. Iwai, Y. Hiyama, K. Suziki, H. Ito, H. Teracuchi, M. Kawasaki, K. Nagai, M. Wachi, J. Yamagishi, J. Med. Chem. 47 (2004) 3693–3696.
[8] P.C. Lv, H.Q. Li, J. Sun, Y. Zhou, H.L. Zhu, Bioorg. Med. Chem. 18 (2010) 4606–4614.
[9] C.Y. Panicker, M.R. Anoop, P.S. Binil, Y.S. Mary, H.T. Varghese, T.K. Manojkumar, Int. J. Ind. Chem. 2 (2011) 33–44.
[10] P.S. Binil, Y.S. Mary, H.T. Varghese, C.Y. Panicker, M.R. Anoop, T.K. Manojkumar, Spectrochim. Acta 94 (2012) 101–109.
[11] Y.S. Mary, C.Y. Panicker, M. Sapnakumari, B. Narayana, B.K. Sarojini, A.A. Al-Saadi, C. Van Alsenoy, J.A. War, H.K. Fun, Spectrochim. Acta 136 (2015) 473–482.
[12] Y.S. Mary, C.Y. Panicker, M. Sapnakumari, B. Narayana, B.K. Sarojini, A.A. Al-Saadi, C. Van Alsenoy, J.A. War, Spectrochim. Acta 136 (2015) 483–493.
[13] Y.S. Mary, C.Y. Panicker, M. Sapnakumari, B. Narayana, B.K. Sarojini, A.A. Al-Saadi, C. Van Alsenoy, J.A. War, H.K. Fun, Spectrochim. Acta 138 (2015) 529–538.
[14] B. Narayana, V.V. Salian, B.K. Sarojini, J.P. Jasinski, Acta Cryst. E70 (2014) o781–o781.
[15] M.J. Frisch, G.W. Trucks, H.B. Schlegel, G.E. Scuseria, M.A. Robb, J.R. Cheeseman, G. Scalmani, V. Barone, B. Mennucci, G.A. Petersson, H. Nakatsuji, M. Caricato, X. Li, H.P. Hratchian, A.F. Izmaylov, J. Bloino, G. Zheng, J.L. Sonnenberg, M. Hada, M. Ehara, K. Toyota, R. Fukuda, J. Hasegawa, M. Ishida, T. Nakajima, Y. Honda, O. Kitao, H. Nakai, T. Vreven, J.A. Montgomery Jr., J.E. Peralta, F. Ogliaro, M. Bearpark, J.J. Heyd, E. Brothers, K.N. Kudin, V.N. Staroverov, T. Keith, R. Kobayashi, J. Normand, K. Raghavachari, A. Rendell, J.C. Burant, S.S. Iyengar, J. Tomasi, M. Cossi, N. Rega, J.M. Millam, M. Klene, J.E. Knox, J.B. Cross, V. Bakken, C. Adamo, J. Jaramillo, R. Gomperts, R.E. Stratmann, O. Yazyev, A.J. Austin, R. Cammi, C. Pomelli, J.W. Ochterski, R.L. Martin, K. Morokuma, V.G. Zakrzewski, G.A. Voth, P. Salvador, J.J. Dannenberg, S. Dapprich, A.D. Daniels, O. Farkas, J.B. Foresman, J.V. Ortiz, J. Cioslowski, D.J. Fox, Gaussian 09, Revision C.01, Gaussian, Inc., Wallingford CT, 2010.
[16] J.B. Foresman, in: E. Frisch (Ed.), Exploring Chemistry with Electronic Structure Methods: a Guide to Using Gaussian, Gaussian Inc., Pittsburg, PA, 1996.
[17] A.D. Becke, J.Chem. Phys. 98 (1993) 5648–5652.
[18] C. Lee, W. Yang, R.G. Parr, Phys. Rev. B 37 (1988) 785–789.
[19] N.C. Handy, P.E. Masley, R.D. Amos, J.S. Andrews, C.W. Murray, G. Laming, Chem. Phys. Lett. 197 (1992) 506–515.
[20] R. Dennington, T. Keith, J. Millam, GaussView, Version 5, Semichem Inc., Shawnee Mission KS, 2009.
[21] J.M.L. Martin, C. Van Alsenoy, GAR2PED, a Program to Obtain a Potential Energy Distribution from a Gaussian Archive Record, University of Antwerp, Belgium, 2007.
[22] N.P.G. Roeges, A Guide to the Complete Interpretation of IR Spectra of Organic Compounds, Wiley, New York, 1994.
[23] N.B. Colthup, L.H. Daly, S.E. Wiberly, Introduction to IR and Raman Spectroscopy, Academic Press, New York, 1990.
[24] R.M. Silverstein, F.X. Webster, Spectrometric Identification of Organic Compounds, sixth ed., John Wiley, Asia, 2003.
[25] G. Socrates, IR Characteristic Group Frequencies, John Wiley and Sons, New York, 1981.
[26] V. Arjunan, I. Saravanan, P. Ravindran, S. Mohan, Spectrochim. Acta 74 (2009) 642–649.
[27] J.S.P.P. Leela, R. Hemamalini, S. Muthu, Int. J. ChemTech. Res. 8 (2015) 203–215.
[28] G. Varsanyi, Assignments of Vibrational Spectra of Seven Hundred Benzene Derivatives, Wiley, New York, 1974.
[29] C.Y. Panicker, K.R. Ambujakshan, H.T. Varghese, S. Mathew, S. Ganguli, A.K. Nanda, C. Van Alsenoy, J. Raman Spectrosc. 40 (2009) 527–536.
[30] J.L. Bredas, C. Adant, P. Tackx, A. Persoons, Chem. Rev. 94 (1994) 243–278.
[31] C. Adant, L. Dupuis, J.L. Bredas, Int. J. Quantum Chem. 56 (2004) 497–507.
[32] C. Hatting, O. Christiansen, P. Jorgensen, Chem. Phys. Lett. 282 (1998) 139–149.
[33] K. Fukui, T. Yonezawa, H. Shingu, J. Chem. Phys. 20 (1952) 722–726.
[34] R.G. Parr, P.K. Chattaraj, J. Am. Chem. Soc. 113 (1991) 1854–1855.
[35] R.G. Parr, L.V. Szentpaly, S. Liu, J. Am. Chem. Soc. 121 (1999) 1922–1924.
[36] R.T. Ulahannan, C.Y. Panicker, H.T. Varghese, R. Musiol, J. Jampilek, C. Van Alsenoy, J.A. War, T.K. Manojkumar, Spectrochim. Acta 150 (2015) 190–199.
[37] A.D. Becke, J. Chem. Phys. 98 (1993) 5648–5652.
[38] P. Thul, V.P. Gupta, V.J. Ram, P. Tandon, Spectrochim. Acta 75 (2010) 251–260.
[39] E.D. Glendening, A.E. Reed, J.E. Carpenter, F. Weinhold, NBO Version 3.1, Gaussian Inc., Pittsburgh, PA, 2003.
[40] G.M. Nitulescu, C. Draghici, O.T. Olaru, Int. J. Mol. Sci. 14 (2013) 21805–21818.
[41] D. Bebbington, H. Binch, J.D. Charrier, S. Everitt, D. Fraysse, J. Golec, D. Kay, R. Knegtel, C. Mak, F. Mazzei, Bioorg. Med. Chem. Lett. 19 (2009) 3586–3592.
[42] G.C. Fletcher, R.D. Brokx, T.A. Denny, T.A. Hembrough, S.M. Plum, W.E. Fogler, C.F. Sidor, M.R. Bray, Mol. Cancer Ther. 1 (2011) 126–137.
[43] A.A. Mortlock, K.M. Foote, N.M. Heron, F.H. Jung, G. Pasquet, J.J. Lohmann, N. Warin, F. Renaud, C. de Savi, N.J. Roberts, J. Med. Chem. 9 (2007) 2213–2224.
[44] A. Balbi, M. Anzaldi, C. Maccio, C. Aiello, M. Mazzei, R. Gangemi, P. Castagnola, M. Miele, C. Rosano, M. Viale, Eur. J. Med. Chem. 46 (2011) 5293–5309.
[45] B. Nyamaa, H.K. Kim, Y.J. Jeong, I.S. Song, J. Han, J. Lipid Atheroscler. 3 (2014) 63–78.
[46] O. Trott, A.J. Olson, J. comput. Chem. 31 (2010) 455–461.
[47] B. Kramer, M. Rarey, T. Lengauer, Proteins Struct. Funct. Genet. 37 (1999) 228–241.
[48] Y.S. Mary, N.R. El-Brollosy, A.A. El-Emam, O.A. Al-Deeb, P.J. Jojo, C.Y. Panicker, C. Van Alsenoy, Spectrochim. Acta 133 (2014) 449–456.
[49] Y.S. Mary, K. Raju, I. Yildiz, O.T. Arpaci, H.I.S. Nogueira, C.M. Granadeiro, C. Van Alsenoy, Spectrochim. Acta 96 (2012) 617–625.